



HAL
open science

Line-shape parameters and their temperature dependences predicted from molecular dynamics simulations for O₂-and air-broadened CO₂ lines

H. T. Nguyen, N. H. Ngo, H. Tran

► **To cite this version:**

H. T. Nguyen, N. H. Ngo, H. Tran. Line-shape parameters and their temperature dependences predicted from molecular dynamics simulations for O₂-and air-broadened CO₂ lines. *Journal of Quantitative Spectroscopy and Radiative Transfer*, 2020, 242, pp.106729. 10.1016/j.jqsrt.2019.106729 . hal-02500553

HAL Id: hal-02500553

<https://hal.sorbonne-universite.fr/hal-02500553>

Submitted on 6 Mar 2020

HAL is a multi-disciplinary open access archive for the deposit and dissemination of scientific research documents, whether they are published or not. The documents may come from teaching and research institutions in France or abroad, or from public or private research centers.

L'archive ouverte pluridisciplinaire **HAL**, est destinée au dépôt et à la diffusion de documents scientifiques de niveau recherche, publiés ou non, émanant des établissements d'enseignement et de recherche français ou étrangers, des laboratoires publics ou privés.

Line-shape parameters and their temperature dependences predicted from molecular dynamics simulations for O₂- and air-broadened CO₂ lines

H. T. Nguyen^{1,2,3}, N. H. Ngo^{1,*} and H. Tran^{2,†}

¹ Faculty of Physics, Hanoi National University of Education, 136 Xuan Thuy, Cau Giay, Hanoi, Vietnam

² Laboratoire de Météorologie Dynamique, IPSL, CNRS, Sorbonne Université, École normale supérieure, PSL Research University, École polytechnique, F-75005 Paris, France

³ REMOSAT, University of Science and Technology of Hanoi (USTH), Vietnam Academy of Science and Technology (VAST)

Abstract

Requantized classical molecular dynamics simulations (rCMDS) were performed for CO₂ highly diluted in O₂ at 200, 250, 296 and 350 K using a site-site intermolecular potential. The simulations were made for 0.5 atm of O₂ pressure and for a large range of Doppler widths, covering near-Doppler regime to collisional-dominant regime. The Fourier-Laplace transform of the auto-correlation functions of the dipole moment, calculated by rCMDS, leads to the associated spectra of CO₂ broadened by O₂. Different effects of collisions between CO₂ and O₂ molecules are included in the simulated spectra. In order to determine the profile parameters of O₂-broadened CO₂ lines, the rCMDS-calculated spectra were fitted with the speed-dependent Nelkin-Ghatak profile associated with the first-order line mixing. The collisional line broadening coefficient, its speed dependence component, the Dicke narrowing and the first-order line-mixing parameters were retrieved for lines with J up to 50 and for all considered temperatures. The temperature dependences of these line-shape parameters were then deduced using the usual single power law. From results obtained in this work and those obtained for CO₂ in N₂ [Nguyen *et al*, *J Chem Phys*, **149**, 224301, 2018], the air-broadened line-shape parameters and their temperature dependences for CO₂ lines were calculated and compared with literature data showing very good agreement.

Keywords: Molecular dynamics simulations, rCMDS, O₂-broadened CO₂, line shape, line mixing, speed-dependent Nelkin-Ghatak profile, speed dependence, Dicke narrowing

1. Introduction

Carbone dioxide (CO₂) is one of the most abundant elements in the Earth's atmosphere, the second greenhouse gas after atmospheric water. Measuring the atmospheric CO₂ columns with high precision and high accuracy in order to understand CO₂ source and sink processes is the objective of several space-born (e.g. [1-4]) experiments. To this aim, an uncertainty below 1 ppm (0.3%) is needed for the retrieved atmospheric CO₂ columns [5,6]. The latter are retrieved by minimizing the difference between the measured spectra and those calculated using a forward model based on the knowledge of the spectroscopy of CO₂ and interfering gases. The precision requirement of atmospheric remote sensing studies thus puts very severe constraints on the quality of the CO₂ spectroscopic data (i.e. line position, line intensity and line profile) needed for the forward calculations. It is now well known that one has to take into account

* Corresponding author: hoa.nn@hnue.edu.vn

† Corresponding author: ha.tran@lmd.jussieu.fr

refined collisional effects on the spectral profile in order to accurately model the measured lines and to achieve the per mill precision requirement of applications (see [7] and references therein). These effects include the collisions-induced line mixing, the molecular speed dependences of the collisional line broadening and shifting, the collisions-induced velocity changes. Many laboratory studies were devoted to the precise determination of line-shape parameters for CO₂ (e.g. [8-14]). In these works, line-shape parameters were generally retrieved from high quality spectra measured under various pressure conditions, using a multi-spectrum fitting procedure [15]. In parallel, it was recently shown that line-shape parameters for linear molecules can be predicted using requantized classical molecular dynamics simulations (rCMDS) [16,17]. Indeed, in these rCMDS, one can simulate the time evolution of a very large number of molecules from an intermolecular potential. The auto-correlation function of the dipole moment, responsible for the optical transition can thus be calculated. The Fourier-Laplace transform of this auto-correlation function directly yields the corresponding absorption spectrum. It was demonstrated in a series of papers that rCMDS are capable to reproduce various collisional effects affecting the absorption spectrum of different molecular systems [16-27]. In a recently published paper [16], rCMDS were used to predict line-shape parameters for N₂-broadened CO₂ lines. To this aim, the rCMDS-calculated spectra of CO₂ in N₂ were fitted with the speed-dependent Nelkin-Ghatak (sdNG) profile in order to retrieve the collisional line broadening coefficient, its speed dependence, the Dicke narrowing and the first-order line-mixing parameters. The predicted parameters were then compared with those determined from high quality measurements [14] showing very good agreement, even for the high-order line-shape parameters [16]. rCMDS are thus a complementary tool for line-shape studies provided that an accurate intermolecular potential is available. Furthermore, the calculations can be performed relatively easily for various temperature conditions, which is not always possible for laboratory measurements. As a follow up to the study of [16], in this paper, rCMDS are used to predict line-shape parameters for O₂-broadened CO₂ lines.

This paper is organized as follows: In Sec. 2 the rCMDS calculations used for CO₂ diluted in O₂ are described as well as the analysis procedure of the simulated spectra. The predicted parameters for O₂-broadened CO₂ but also for CO₂ in air, computed from those of CO₂ in O₂ and of CO₂ in N₂ are presented and compared with literature data in Sec. 3 while the conclusion and perspectives of this work are summarized in Sec. 4.

2. Classical molecular dynamics simulations for CO₂-O₂ and analysis procedure

Calculations were made for four temperatures 200, 250, 296 and 350 K at 1 atm for CO₂-O₂ mixtures with 50% of CO₂ using the IBM Blue Gene/P computer of the *Institut du Développement et des Ressources en Informatique Scientifique* but also the facilities of the faculty of physics at Hanoi National University of Education. Only CO₂-O₂ interactions being taken into account, this is equivalent to CO₂ infinitely diluted in 0.5 atm of O₂. Details on the calculations method can be found in [16] and references therein. A site-site functional form with Coulombic and atom-atom contributions was used to describe the interaction potential between CO₂ and O₂ molecules. For that, the molecular geometries, the charges and sites were taken from [28] and [29] for CO₂ and O₂, respectively. The atom-atom contribution was calculated as a 12-6 Lennard-Jones potential whose parameters were deduced using usual combination laws [30] and parameters for CO₂-CO₂ [28] and O₂-O₂ [29] interactions. These potentials for CO₂-CO₂ and O₂-O₂ were successfully used to predict non-Voigt effects on the line shapes of pure CO₂ (e.g. [19]) and O₂ in air (e.g. [17]), respectively. The molecules were considered as rigid rotors and all the effects of vibrational motion were disregarded in the calculations. Note that our rCMDS do not take into account the dephasing of the dipole, which

is associated with the fact that the effects of intermolecular interactions for molecules in the upper and lower states of the optical transitions are different. Consequently, the calculated spectra do not show any pressure shift.

For each temperature, a total number of about 3×10^8 molecules was considered. The molecules were treated in parallel in more than fifteen thousand boxes, each containing 20 000 molecules. The molecules were randomly initialized in the boxes with translational and angular speeds verifying the Maxwell-Boltzmann distribution. Random center-of-mass velocity vector and molecular axis orientation were attributed. The parameters (center-of-mass position, velocity, angular momentum, and molecular orientation) describing the classical state of each molecule were then computed for each time step. A requantization procedure, as done in [16,18] for pure CO₂ and for CO₂ in N₂, was applied to the classical rotation of the molecules. Specifically, for a molecule of rotational angular speed ω , we find the (even) integer J for which $\hbar J/I$, where I is the moment of inertia, is the closest to ω . This corresponds to matching the classical rotational frequency with the quantum position of the P branch lines. Once J is found, ω is requantized by applying the change $\omega = \hbar J/I$ while the orientation of the rotational angular momentum is kept unchanged. This P branch requantization implies that the calculated R branch spectrum will be the exact symmetric of the P branch. The auto-correlation function of the dipole moment, assumed along the molecular axis (as the case for the asymmetric stretching absorption bands of CO₂, for instance), was then calculated during the requantized CMDS (rCMDS). The Doppler effect associated to the translational motion was taken into account in this auto-correlation function. For each temperature, eight values of the Doppler width Γ_D (ranging from about 0.002 cm⁻¹ to 0.3 cm⁻¹) were used in the calculations. This provided a large set of values of the ratio Γ_L/Γ_D (from about 0.08 to 13, Γ_L being the Lorentz width), covering a range from the near purely Doppler to collision-dominant regimes. Since all the effects of vibrational motion were disregarded in our rCMDS, this corresponds to eight calculations at eight values of pressure with a unique Doppler width. Finally, the absorption coefficient was obtained as the Fourier-Laplace transform of the auto-correlation function of the dipole moment. The spectra were thus calculated without the use of any adjustable parameter.

rCMDS were also performed for CO₂ in N₂ at 250 K, using the same calculations procedure as in our previous work devoted to CO₂/N₂ [16]. In the latter, only two temperature conditions were considered, i.e. 200 and 296 K. The use of this calculation in addition to those of [16] allows to improve the precision of the predicted temperature dependences of CO₂/N₂ line-shape parameters. The results obtained for CO₂/N₂ and those for CO₂/O₂ will be used in this work to deduce the air-broadened CO₂ line-shape parameters and their temperature dependences.

As for the case of CO₂/N₂ [16], the rCMDS-calculated spectra for each temperature were fit with the speed-dependent Nelkin-Ghatak (sdNG) profile including the first-order line mixing [31]. As well known (see [32] and references therein), this profile takes into account the Doppler effect, the collisional broadening, its speed dependence and the collisions-induced velocity changes. For each considered temperature, the Doppler broadening Γ_D is fixed to values used in the rCMDS. The speed-dependent collisional half-width, $\Gamma(v)$, is modeled using the quadratic law [33,34], i.e. $\Gamma(v) = \Gamma_0 + \Gamma_2[(v/\tilde{v})^2 - 3/2]$ in which $\tilde{v} = \sqrt{2k_B T/m}$ is the most probable speed for an absorbing molecule of mass m . The (thermally averaged) line width, Γ_0 and its speed dependence component, Γ_2 , both in cm⁻¹, are adjusted in the fits. The collision-induced velocity changes (VC) effect is taken into account by using the hard-collision model [35,36]. Within this model, this effect is characterized by the velocity changing collisions rate ν_{vc} (or the Dicke narrowing frequency, in cm⁻¹) which will be retrieved from the fits. Finally, the first-order line-mixing parameter, Y (no unit) accounting for the coupling between the considered line and the others, is also adjusted in the fits.

A multi-spectrum fitting procedure, developed previously in our group (e.g. [37,38]) was used to retrieve the line-shape parameters. For a given temperature, spectra of the same line, calculated for various Doppler width values, were simultaneously adjusted, the line-shape parameters being constrained to be the same for all spectra. As mentioned previously, the pressure-shifting was fixed to zero since no pressure shift was taken into account in our rCMDS. For each line, the line-broadening coefficient γ_0 (Γ_0/P , in $\text{cm}^{-1}/\text{atm}$), its speed dependence component γ_2 (Γ_2/P , in $\text{cm}^{-1}/\text{atm}$), the Dicke narrowing parameter β (v_{vc}/P , in $\text{cm}^{-1}/\text{atm}$) and the first-order line-mixing coefficient $\zeta(Y/P$, in atm^{-1}) were retrieved for each temperature. Their temperature dependences were then represented by the usual power law, i.e. $A(T) = A(T_0)(\frac{T_0}{T})^{n_A}$, in which $T_0 = 296$ K and $A(T)$ is either γ_0 , γ_2 , β or ζ and n_A is the temperature dependence exponent. The obtained results are presented in the next section.

3. Results and discussions

Figure 1 shows the simulated spectra of CO_2 in O_2 for the P(10) and P(20) lines for three different values of Γ_L/Γ_D and at 200 and 296 K respectively. Residuals obtained from fitting these spectra with various line-shape models are shown in the lower panels. In addition to the sdNG profile, tests were also performed with more simplified models: the speed-dependent Voigt (sdV) (no Dicke narrowing effect), the Nelkin-Ghatak (NG) (no speed dependence effect) and the widely used Voigt (V) profiles. For all the used line profiles, line-mixing effect was taken into account. As can be observed on the examples of Fig. 1, the Voigt profile leads to the worse fits, with magnitude of fit residuals up to 3%. The NG profile is in better agreement with the calculated spectra but significant structures remain in the fit residuals. Better fit residuals are obtained with the sdV and sdNG profiles. The remaining residuals are mainly due to the numerical noises in the rCMDS calculations. With respect to the sdV profile, the sdNG profile leads to slightly better residuals. This will explain the smallness and the large uncertainty of the retrieved Dicke narrowing parameters, presented in Sec. 3.3. Tests were also made with the Hartmann-Tran profile [32,39] in which the correlation between velocity changes and internal state changes is also taken into account. However, the results show no improvement with respect to the sdNG profile. The sdNG model is thus retained for the analysis of the simulated spectra, as for the case of CO_2 in N_2 [16]. The retrieved line-shape parameters and their temperature dependences will be presented and compared with literature data in the next subsections.

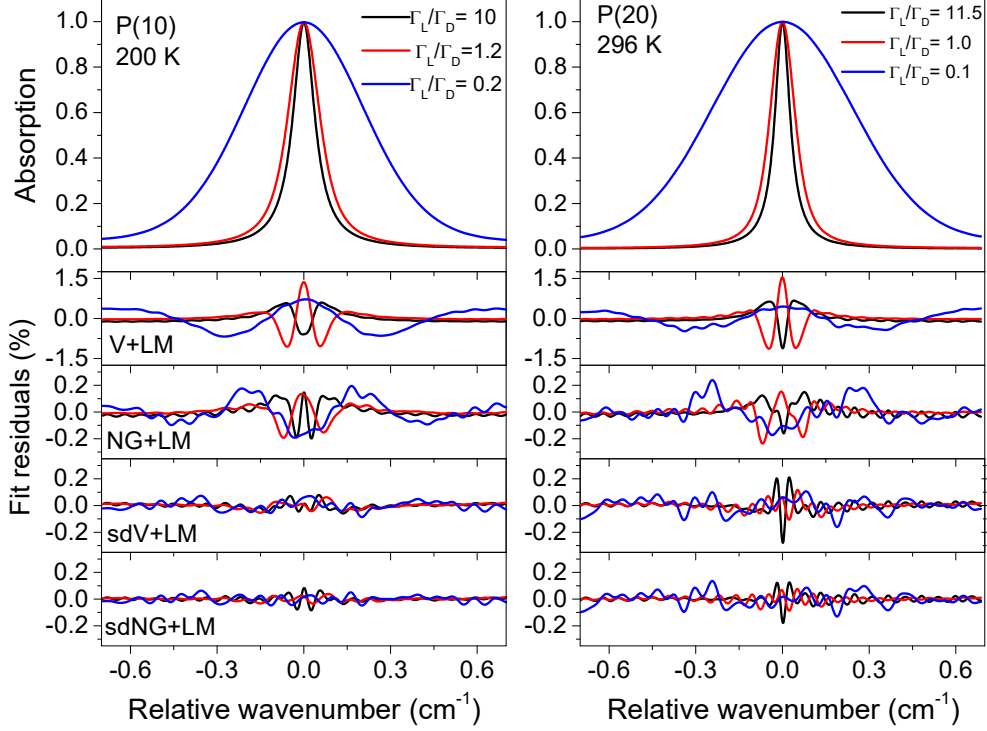


Fig. 1: rCMDS-calculated spectra for the P(10) and P(20) lines of CO₂ broadened by O₂ at 200 K and 296 K, respectively and for different Γ_L/Γ_D ratios, the O₂ pressure being 0.5 atm. In the lower panels are the fit residuals obtained from multi-fitting these spectra with the Voigt (V), the Nelkin-Ghatak (NG), the speed-dependent Voigt (sdV) and the speed-dependent Nelkin-Ghatak (sdNG) profiles. Line-mixing effect was taken into account using the first-order approximation.

3.1 The line-broadening coefficient and its temperature dependence

The retrieved broadening coefficients for O₂-broadened CO₂ lines are presented in the right part of Fig. 2 versus the rotational quantum number $|m|$ ($m = -J$ for P branch lines, J being the rotational quantum number of the lower level of the line) for the four considered temperatures. Due to their weak signal-to-noise ratio, broadening coefficient for lines with $|m|$ greater than 60 could not be determined. Several studies in the literature were devoted to the measurements of the O₂-broadening coefficients of CO₂ lines (see [40] and references therein). Most of them employed the Voigt profile to model the measured spectra, except [40] and [41]. In [40], the speed-dependent Voigt profile was used to retrieve the O₂-broadened CO₂ line-shape parameters in the 30013←00001 and 30012←00001 bands from high-resolution FTS spectra of CO₂ lines. Hikida and Yamada [41] used the Galatry profile to determine O₂-broadening coefficients for ten CO₂ lines in the 30013←00001 band from diode laser measurements. It is well known that using the Voigt profile leads to smaller retrieved line broadening coefficients with respect to more refined line-shape models. Therefore, only [40] and [41] are retained here for comparison with our predicted results (left part of Fig. 2), both the measured and calculated values were obtained at room temperature. As can be observed, our predicted values are in rather good agreement with measured results, with an average difference of about 2%, a very satisfying result for a classical method.

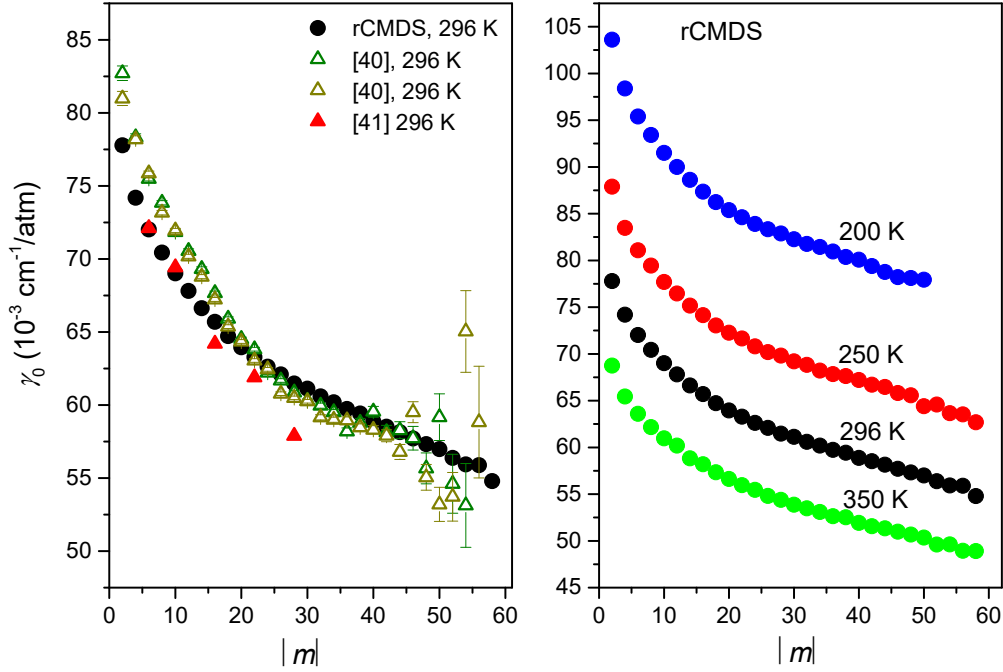


Fig. 2: Left panel: O_2 -broadening coefficients of CO_2 lines deduced from fits of rCMDS-calculated spectra at 296 K (black circles) with the sdNG profile and comparison with measured values of [40] (olive and dark yellow triangles for the 30012 \leftarrow 00001 and 30013 \leftarrow 00001 bands, respectively) and [41] (red triangles) (see text).

Right panel: rCMDS-predicted broadening coefficients of CO_2 in O_2 at 200, 250, 296 and 350 K.

The predicted broadening coefficients for CO_2/O_2 at 200, 250 and 296 K are then combined with those of CO_2/N_2 at the same temperature conditions (from [16] and this work) to deduce the air-broadening coefficients using $\gamma_0^{air}(T) = 0.79\gamma_0^{N_2}(T) + 0.21\gamma_0^{O_2}(T)$. Note that the fact that $\gamma_0^{N_2}$ are larger than $\gamma_0^{O_2}$ is well reproduced by rCMDS predictions (see also Fig. 2 of [16]). Figure 3 shows the obtained air-broadening coefficients for the three considered temperatures and their comparison with data of [11], [13] and of [12,42]. In those studies, air-broadening coefficients were determined from fits of measured spectra using the sdNG [13], the partially-correlated speed-dependent Nelkin-Ghatak (pcsdNG) [11] and the sdV [12,42] profiles. We can reasonably compare values of γ_0 obtained with these various speed-dependent profiles since, as demonstrated in [9,43], the differences between values of γ_0 obtained with these speed-dependent profiles are very small, below 1%. In [13] only the R(16) line of the 30013 \leftarrow 00001 band was measured but for various temperatures. Values of γ_0 for 36 lines in the 30012 \leftarrow 00001 band were measured in [11] at room temperature. In [12], lines of various vibrational bands in the 2.06 μm spectral region were measured at various temperatures, only parameters of the most intense band (20013 \leftarrow 00001) being shown here. Finally, [42] was devoted to the (30013 \leftarrow 00001) band of CO_2 . Values of [13] and [12,42] at 250 and 200 K were deduced from the coefficients given at room temperature and the temperature dependence exponents. As shown in Fig. 3, a very good agreement between our predictions and these data can be observed. Most of the measured data are in good agreement with the predictions, except for values at low $|m|$ where the difference between our prediction and measured values of [12] can be up to 5%. These results confirms the quality of predictions using requantized CMDS and the associated intermolecular potential.

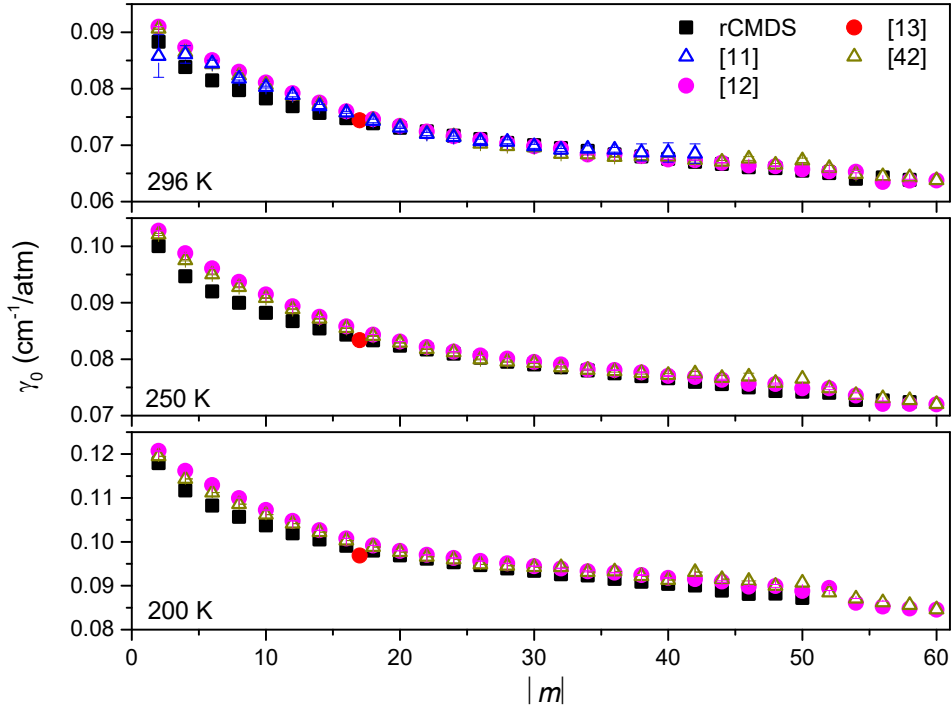


Fig.3: Air-broadening coefficients predicted by rCMDS using results obtained here for O₂-broadening and those for N₂-broadening obtained in [16] and in this study, at 296, 250 and 200 K. Results of [13], [11], and [12,42], obtained from fits of measured spectra with respectively, the sdNG, pcsdNG and sdV profiles, are also displayed for comparison.

The temperature dependences for O₂- and air-broadening coefficients are determined using the usual power law (see Sec.2). The obtained results are displayed in Fig. 4, together with data for CO₂/air of [13] and [12,42] but also those given in the 2016 edition of the HITRAN database [44]. For completeness, experimental values of [14] for N₂-broadened CO₂ lines in the ν_3 band, obtained with the use of the sdNG profile, are also reported. For the predicted values, error bars obtained from the standard uncertainty of the fits (1σ) for the temperature exponents are also displayed. As can be seen on Fig. 4, our predicted values for O₂ and air-broadening are quite close to each other, the maximum difference being for high $|m|$. For air-broadening, all the plotted data including the predicted ones are in good agreement, within 7-8%. This demonstrates that rCMDS can be fully used to predict the temperature dependences of the broadening coefficients for molecular systems such as CO₂. The rCMDS predicted values of $\gamma_0(296\text{ K})$ and n_{γ_0} are listed in Table 1 and 2 for O₂- and air-broadening, respectively.

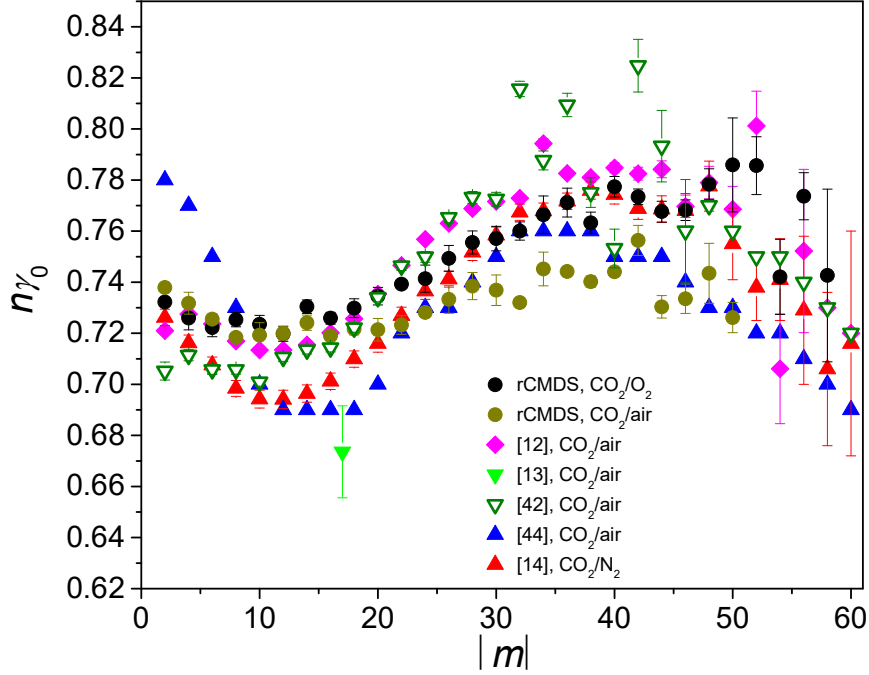


Fig. 4: The temperature exponents of O₂- (black circles) and air-broadening (olive circles) coefficients of CO₂, deduced from rCMDS and comparison with those for CO₂ in air of [12] (purple diamonds), [13] (green triangles), [42] (olive triangles) and [44] (blue triangles) and for CO₂ in N₂ of [14] (red triangles).

3.2. The speed dependence of the line width and its temperature dependence

Results for the predicted speed dependence parameters γ_2 for O₂- but also for air-broadening are presented in Fig. 5 for all considered temperatures. The ratios γ_2/γ_0 is plotted instead of γ_2 . This allows for a straightforward comparison with literature data, since most of papers directly give this ratio. By combining the statistical uncertainty obtained from the fits and that due to the fitting technique (i.e. by changing the spectral range of the fits), we estimate a total uncertainty (1σ) of 5% for γ_2 . Our results are compared with those of [40] for O₂-broadening and of [11-13,42] for air. In [11], the ratio γ_2/γ_0 for air-broadening was assumed to be independent of the line (i.e. of m) and was obtained from fits of measured spectra of the R(16) line of the 30012←00001 band [10] with the pcsdNG profile at room temperature. The comparison in Fig. 5 shows that at $|m| = 17$, the value of [11] is in good agreement with our result at room temperature but assuming γ_2/γ_0 independent of m is probably too simplified. In [13], the same line but for the 30013←00001 band was investigated at various temperatures, using the sdNG profile. The retrieved value of γ_2/γ_0 , independent of T, is also in very good agreement with our predictions. Large differences with our results are observed when comparing to [12,42] for CO₂ in air and to [40] for CO₂ in O₂. These differences are due to the different line-shapes used in [12,40,42] and in our work. [12,40,42] used the speed-dependent Voigt profile while the speed-dependent Nelkin-Ghatak profile is used in the present work to retrieve line-shape parameters. The speed dependence parameter obtained with the sdV profile is usually larger than that obtained using the sdNG or HT profile, as observed in [38,43,45,46] for instance. Note that in [12,40,42], the ratio γ_2/γ_0 was assumed to be independent of T, as in [13]. As shown in Fig. 5, the ratios γ_2/γ_0 predicted by rCMDS at different temperatures are quite close each other. This demonstrates that the temperature dependence of γ_2/γ_0 for O₂ and air-broadening CO₂ lines is relatively weak. In Refs. [13,43], it was shown that within the quadratic approximation for the speed-dependent broadening and the power law for the

temperature dependence of the line broadening coefficient, γ_2/γ_0 is independent of temperature and can be given by [13]

$$\frac{\gamma_2}{\gamma_0} = (1 - n) \frac{2}{3} \frac{\frac{m_p}{m_a}}{1 + \frac{m_p}{m_a}} \quad (1)$$

In this equation, n is the temperature exponent of γ_0 and m_a , m_p are respectively the masses of the absorbing and perturbing molecules. The values of n (Fig. 4) predicted by rCMDS were thus used to deduce γ_2/γ_0 using this relation. The obtained results for O₂- and air-broadening are shown in Fig. 5. As can be observed, it leads to rather good agreement with rCMDS results for CO₂/O₂ but for CO₂/air, Eq. (1) slightly underestimates the values of γ_2/γ_0 predicted by rCMDS.

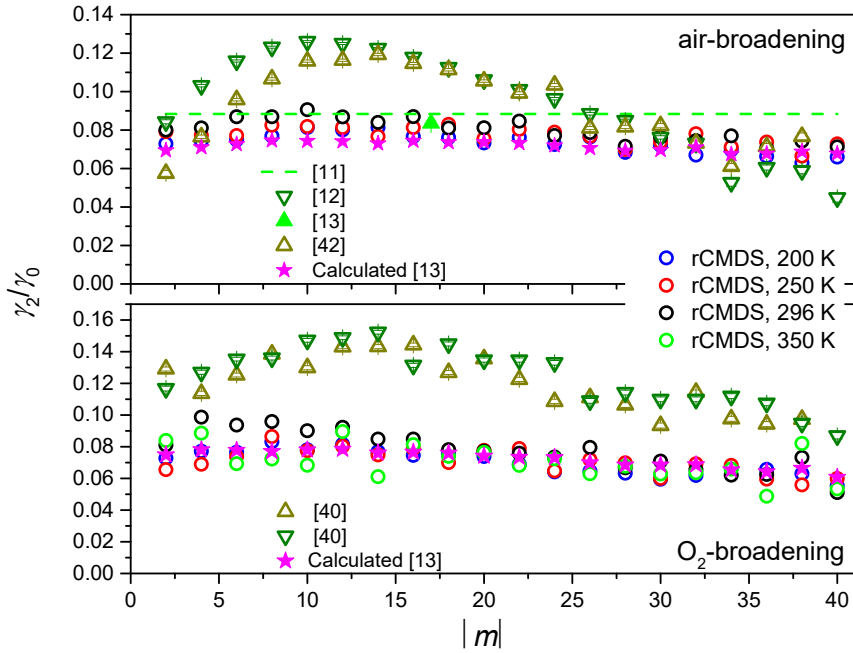


Fig. 5: Bottom panel: the ratio γ_2/γ_0 predicted by fitting the rCMDS-calculated spectra of CO₂/O₂ with the sdNG profile, obtained at 200 K, 250 K, 296K and 350K and comparison with the temperature-independent values of [40] (olive and dark yellow triangles) obtained from fits of measured spectra with the sdV profile. The temperature-independent values, calculated using Eq. (1) [13] and our temperature exponents (magenta stars) are also shown.

Top panel: the rCMDS-predicted γ_2/γ_0 values for CO₂/air, associated with the sdNG profile and comparison with experimental values of [11] (dash green line), [13] (green triangle) and [12,42] (green and dark yellow triangles) obtained respectively with the pcsdNG, sdNG and sdV profiles. The temperature-independent values, calculated using Eq. (1) [13] and our temperature exponents (magenta stars) are also shown.

As for γ_0 , the temperature dependences for γ_2 are also modeled by the power law. From values of γ_2 predicted by rCMDS at various temperatures, n_{γ_2} for O₂- and air-broadening are thus deduced and plotted in Fig. 6, together with their statistical uncertainty obtained from the fits. For comparison, the rCMDS-predicted values for n_{γ_0} (see Fig. 4) are also displayed. For O₂-broadening, the values of n_{γ_2} are determined with large uncertainty and randomly vary between the 0.05-1.2 range. For air-broadening, the variation with $|m|$ of n_{γ_2} is much less random. It is clearly shown that for CO₂ in air, the temperature dependence of γ_2 is weaker than that of γ_0 , which is consistent with the observation of [14] for CO₂ in N₂. This difference with Eq. (1) shows the limit of the phenomenological quadratic speed dependence and probably also of the

power law for the temperature dependence. These models should thus be considered as effective with different temperature dependences for γ_0 and γ_2 .

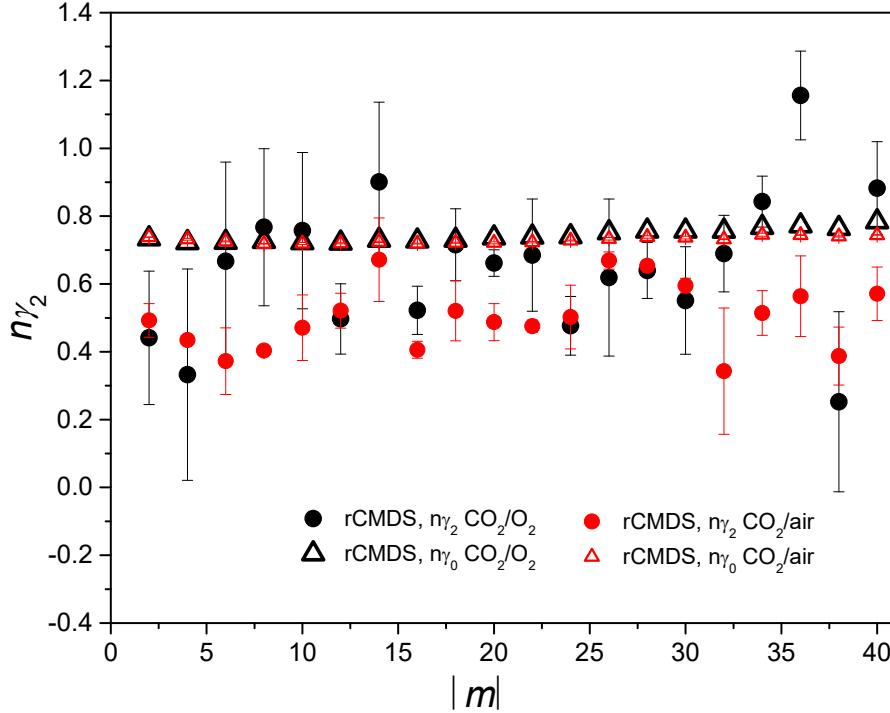


Fig. 6. The temperature exponents of the speed dependence parameters, n_{γ_2} , for O_2 - (red circles) and air-broadened (black circles) CO_2 . n_{γ_0} are also displayed for comparison. The plotted error bars correspond to the uncertainty (1σ) obtained from the fits of the temperature exponents.

3.3 The Dicke narrowing parameter and its temperature dependence

The retrieved Dicke narrowing parameters, β , for all the considered temperatures are presented in the left panel of Fig. 7 for both CO_2/O_2 and CO_2/air . Recall that results for CO_2 in air were determined from results for CO_2/O_2 obtained in this work and those for CO_2/N_2 , from this work and from [16]. It is well known that the Dicke narrowing coefficient strongly depends on the line-shape model used to fit the measured/simulated spectra. For the same line, values obtained with the Nelkin-Ghatak, the speed-dependent Nelkin-Ghatak and the partially-correlated speed-dependent Nelkin-Ghatak profiles could be completely different. To the best of our knowledge, there is no available data for β , obtained with the sdNG profile for O_2 - and air-broadened CO_2 , except [13] in which no value of β can be found. The rCMDS-predicted values of β (left panel of Fig. 7) are rather small compared to those of γ_0 and γ_2 . In fact, as can be observed in Fig. 1, including the Dicke narrowing effect improves only slightly the fit residuals. The determined values are small and largely influenced by the signal to noise ratio of the calculated spectra. The 1σ combined uncertainty for β is about 10-20%. As a consequence, the deduced temperature dependence of the Dicke narrowing parameter, n_β , is associated with large error bars (right panel of Fig. 7). The values of n_β from [14], determined from fits of measured spectra with the sdNG profile, but for CO_2/N_2 are also reported here for comparison.

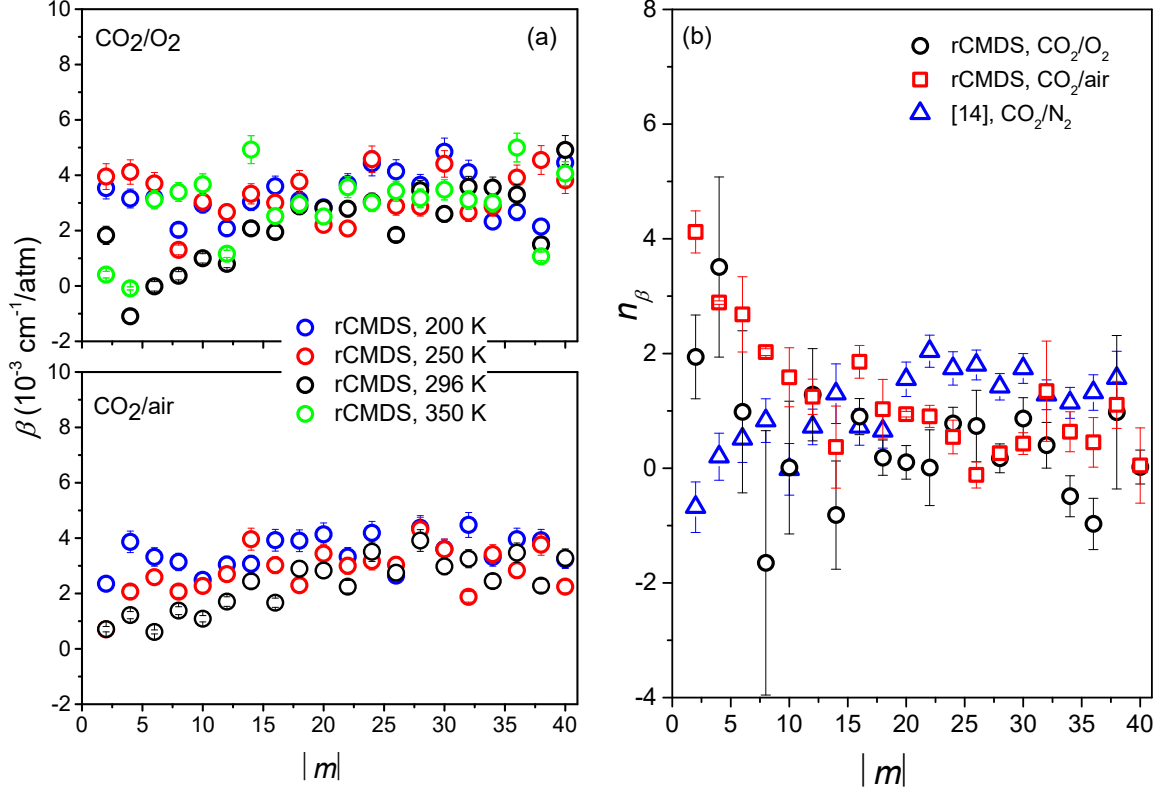


Fig. 7: Left panel: the rCMDS-predicted Dicke narrowing parameters for O_2 and air-broadened CO_2 for all the considered temperatures.

Right panel: the deduced temperature exponents of the Dicke narrowing parameters for O_2 - and air-broadened CO_2 lines and comparison with measurement-deduced values of [14] for CO_2/N_2 .

4.4. The first-order line-mixing parameter and its temperature dependence

Line-mixing effect in CO_2 spectra is of great importance for applications such as atmospheric remote sensing studies (see [47,48] for instance). Various studies were devoted to the calculations and/or measurements of either the first-order line-mixing coefficients or the off-diagonal elements of the relaxation matrix for CO_2 (e.g. [11,12,14,42,48]). The rCMDS predicted first-order line-mixing parameters, ζ , for O_2 -broadened CO_2 for the four considered temperatures are plotted in the left part of Fig. 8. For air-broadened CO_2 , the values of ζ were determined as a combination of those for O_2 - and N_2 -broadening [16] and are shown in the right part of Fig. 8. Our predicted values are compared with measured values of [49] for the 30012←00001 and 30013←00001 bands, obtained with the sdV profile and with those of [11] for the 30012←00001 band, with the pcsdNG profile. The first-order line-mixing parameters deduced from the modeled relaxation matrix of [48] at 296 and 200 K for the ν_3 band are also displayed for comparison. For $|m| \leq 30$ a very good agreement with the measured values is observed while for higher values of $|m|$, the rCMDS-predicted values are larger than the measured and calculated values. Note that the difference with measured values cannot be explained by the difference in the used line profiles since it was observed that the first-order line-mixing parameter does not significantly depend on the line shape (see [38,49] for instance). A possible source of difference could be our requantization scheme. In fact, in the requantization procedure used in our CMDS, we did not take into account the centrifugal distortion effect. As a result, the successive $P(J)$ lines are equally spaced in the rCMDS-calculated spectra, which is not the case for a vibrational band of CO_2 . Furthermore, as

explained in [18], the requantization is based on a single P line criterion. As a result, the calculated R branch spectrum is the exact symmetric of the P branch. We thus disregarded the direction in which molecules rotate, the line-mixing process can be badly taken into account.

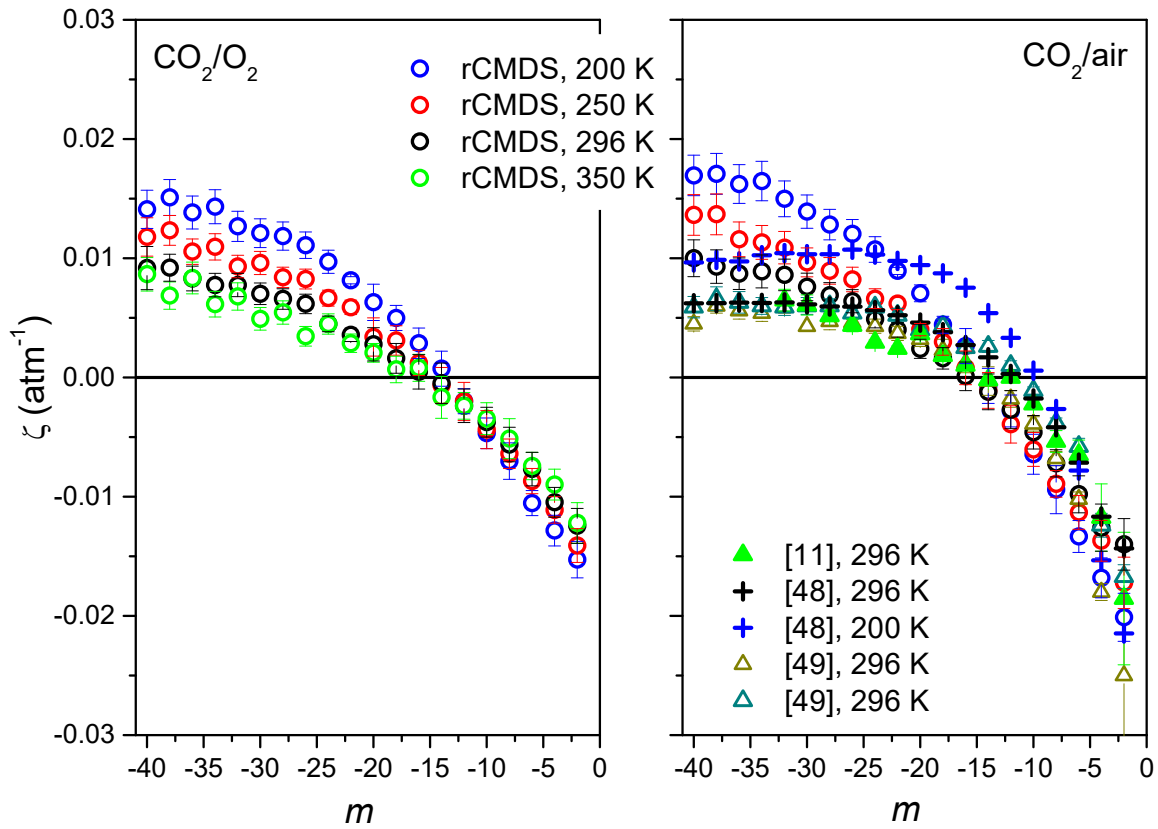


Fig.8: Left panel: first-order line-mixing parameters predicted from rCMDS for O₂-broadened CO₂ at 200, 250, 296 and 350 K.

Right panel: air-broadened first-order line-mixing parameters for CO₂, calculated from the present rCMDS-predicted values for CO₂/O₂ and those of CO₂/N₂ [16] at 200, 250 and 296 K. Measured values for CO₂ in air of [49] for the 30012←00001 (dark cyan) and 30013←00001 (dark yellow) bands, obtained with the *sdV* profile and those of [11] for the (30012←00001) band, with the *psdNG* profile are reported for comparison. Values deduced from the modeled relaxation matrix of [48] for the ν_3 band at 296 and 200 K are also displayed.

The temperature dependence of the rCMDS-predicted ζ is presented in Fig. 9 for both CO₂/O₂ and CO₂/air. The plotted error bar is the uncertainty due to the fit of the temperature exponents which take the uncertainty of $\zeta(T)$ into account. As can be observed, there is no significant difference between n_ζ for O₂- and air-broadening and they are in good agreement with the experimental values of [14] for CO₂ in N₂.

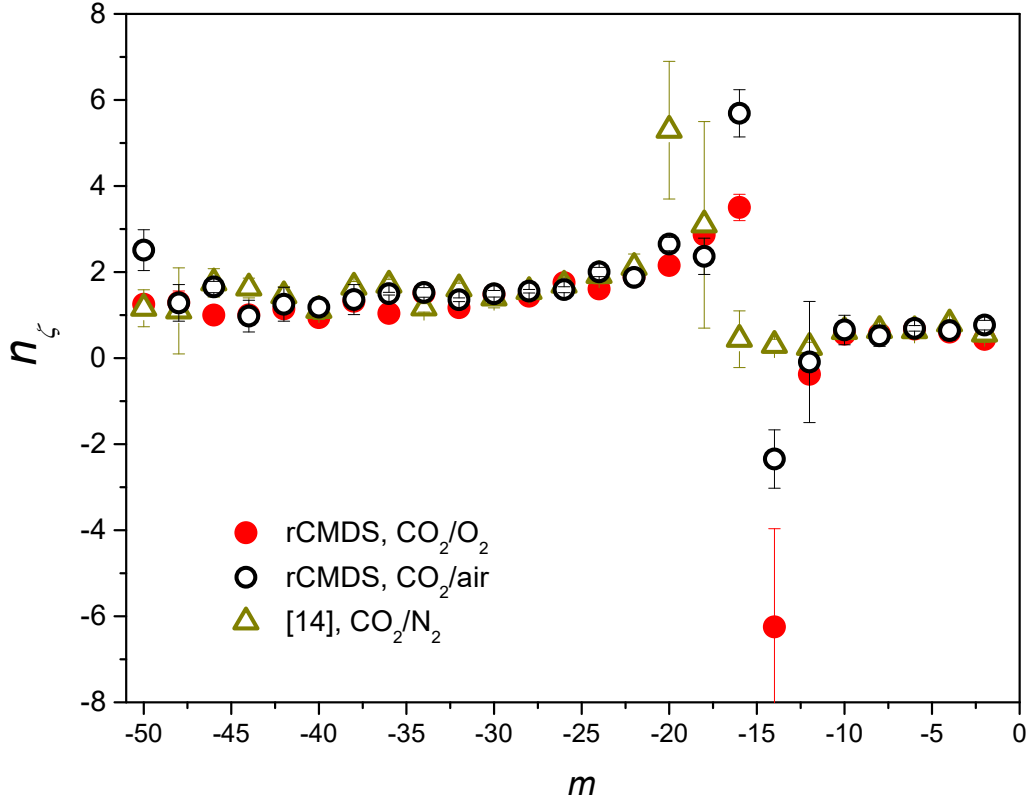


Fig.9: The temperature dependences of the first-order line-mixing parameters predicted by rCMDS for CO₂/O₂ and CO₂/air. Values of [14] for CO₂/N₂ are also displayed for comparison.

5. Conclusions

Line-shape parameters for O₂-broadened CO₂ transitions were predicted using requantized classical molecular dynamics simulations. Spectra were simulated for four temperature conditions, from the near Doppler regime to the collisional one. The various collisional effects affecting the line profile are thus included in the simulated spectra. Line-shape parameters were deduced by fitting the simulated spectra with the quadratic speed-dependent Nelkin-Ghatak profile. The collisional broadening coefficient, its speed dependence, the Dicke narrowing and the first-order line-mixing parameters were retrieved using a multi-spectrum fitting procedure. The temperature dependences of these parameters were obtained using the usual single power law. The obtained parameters for CO₂/O₂ were then combined with those of CO₂/N₂, predicted using rCMDS in our previous study [16] to deduce parameters for CO₂ in air. Comparison of the predicted parameters, their temperature dependences for both CO₂/O₂ and CO₂/air with measured data show very good agreement. This shows that rCMDS can be used as a powerful tool, complementary to high quality measurements, to address the precision and accuracy requirements of application such as atmospheric remote sensing as well as for populating spectroscopic databases with refined line-shape parameters.

Acknowledgments

This work was granted access to the HPC resources of IDRIS under the allocation 2019-A0060907520 made by GENCI. The authors from Hanoi National University of Education (HNUE) are pleased to acknowledge the financial support of this research by the National

Foundation for Science and Technology Development (NAFOSTED) of Vietnam under grant number of 103.03-2018.09.

<i>Line</i>	γ_0	<i>unc</i>	γ_2	<i>unc</i>	β	<i>Unc</i>	ζ	<i>unc</i>	n_{γ_0}	<i>unc</i>	n_{γ_2}	<i>unc</i>	n_β	<i>unc</i>	n_ζ	<i>unc</i>
P2	0.0778	3.8	0.0063	3.2	0.0018	3.3	-0.0124	14.5	0.732	1.6	0.441	196	1.940	730	0.436	57
P4	0.0742	3.7	0.0073	3.7	-0.0011	2.4	-0.0105	12.6	0.726	4.6	0.333	312	3.508	1571	0.603	49
P6	0.0720	3.6	0.0068	3.4	0.0000	1.7	-0.0077	14.1	0.722	3.6	0.667	292	0.983	1413	0.675	80
P8	0.0704	3.5	0.0068	3.4	0.0004	1.5	-0.0056	14.5	0.725	2.8	0.767	231	-1.651	2305	0.562	41
P10	0.0690	3.5	0.0062	3.1	0.0010	1.7	-0.0038	12.5	0.724	3.5	0.757	230	0.011	1156	0.558	71
P12	0.0678	3.4	0.0063	3.1	0.0008	1.3	-0.0024	14.0	0.720	3.0	0.497	104	1.282	804	-0.375	124
P14	0.0666	3.3	0.0057	2.8	0.0021	2.3	-0.0005	17.0	0.730	2.6	0.901	235	-0.817	943	-6.247	2281
P16	0.0657	3.3	0.0056	2.8	0.0020	2.4	0.0005	14.5	0.726	2.3	0.522	71	0.899	314	3.503	306
P18	0.0647	3.2	0.0051	2.5	0.0029	3.0	0.0016	12.5	0.730	3.7	0.716	106	0.184	308	2.865	192
P20	0.0640	3.2	0.0049	2.5	0.0028	2.9	0.0028	13.8	0.734	3.4	0.662	39	0.103	293	2.151	143
P22	0.0633	3.2	0.0048	2.4	0.0028	2.9	0.0036	5.6	0.739	1.7	0.685	166	0.009	660	1.894	125
P24	0.0626	3.1	0.0046	2.3	0.0030	3.1	0.0045	6.5	0.741	5.3	0.477	87	0.779	283	1.609	153
P26	0.0621	3.1	0.0049	2.5	0.0018	2.1	0.0062	8.2	0.749	5.1	0.619	231	0.735	623	1.752	168
P28	0.0615	3.1	0.0041	2.1	0.0035	3.6	0.0066	8.6	0.756	4.5	0.640	83	0.172	251	1.440	40
P30	0.0611	3.1	0.0043	2.2	0.0026	2.9	0.0070	9.1	0.757	4.8	0.551	158	0.866	362	1.478	124
P32	0.0606	3.0	0.0040	2.0	0.0036	3.8	0.0078	9.8	0.760	3.6	0.690	113	0.401	399	1.173	65
P34	0.0602	3.0	0.0037	1.9	0.0036	3.8	0.0078	9.8	0.766	7.4	0.843	75	-0.489	358	1.505	80
P36	0.0597	2.9	0.0037	1.9	0.0033	3.6	0.0083	10.4	0.771	5.7	1.156	131	-0.971	447	1.038	136
P38	0.0594	2.9	0.0044	2.2	0.0015	2.4	0.0092	11.3	0.763	4.2	0.253	266	0.976	1339	1.322	113
P40	0.0589	2.9	0.0030	1.6	0.0049	5.2	0.0092	18.1	0.777	4.0	0.883	137	0.020	295	0.942	88
P42	0.0585	2.9	0.0034	1.7	0.0037	4.1	0.0103	12.4	0.773	3.1	0.927	156	-0.751	797	1.146	110
P44	0.0582	2.9	0.0031	1.7	0.0046	5.0	0.0094	11.5	0.768	4.1	0.405	568	1.476	1608	1.003	175
P46	0.0577	2.9	0.0034	1.7	0.0034	4.1	0.0113	13.5	0.768	4.0	-0.083	1131			0.999	186
P48	0.0573	2.9	0.0032	1.7	0.0040	4.8	0.0094	11.6	0.778	5.9	0.335	368	0.158	993	1.293	267
P50	0.0570	2.9	0.0031	1.7	0.0053	6.2	0.0109	13.1	0.786	18.4	0.863	942	0.224	3603	1.249	175

Table 1: Line-shape parameters for O₂-broadened CO₂ lines, deduced from rCMDS-calculated spectra. γ_0 , γ_2 , β are in cm⁻¹/atm and ζ in atm⁻¹. *Unc* is the total uncertainty (1σ), in units of the last quoted digit.

<i>Line</i>	γ_0	<i>unc</i>	γ_2	<i>unc</i>	β	<i>unc</i>	ζ	<i>unc</i>	n_{γ_0}	<i>unc</i>	n_{γ_2}	<i>unc</i>	n_β	<i>unc</i>	n_ζ	<i>unc</i>
P2	0.0883	4.4	0.0071	3.5	0.0007	0.7	-0.0140	21.7	0.738	0.5	0.484	49.5	3.989	366	0.767	111
P4	0.0838	4.2	0.0068	3.4	0.0012	1.2	-0.0126	19.8	0.732	4.3	0.515	1.0	2.367	30	0.640	219
P6	0.0815	4.1	0.0071	3.5	0.0006	0.6	-0.0098	15.5	0.726	2.0	0.374	98.3	2.683	656	0.689	62
P8	0.0798	4.0	0.0069	3.5	0.0014	1.3	-0.0072	11.4	0.718	1.1	0.406	0.5	1.996	594	0.517	243
P10	0.0783	3.9	0.0071	3.5	0.0011	1.0	-0.0046	14.0	0.719	4.9	0.472	96.8	1.501	515	0.653	342
P12	0.0769	3.8	0.0067	3.3	0.0017	1.7	-0.0027	16.0	0.720	2.5	0.532	51.6	1.151	308	-0.089	1408
P14	0.0757	3.8	0.0064	3.2	0.0024	2.4	-0.0012	15.0	0.724	3.0	0.694	123.3	0.259	716	-2.345	680
P16	0.0748	3.7	0.0065	3.2	0.0017	1.7	0.0001	12.0	0.719	1.9	0.403	24.9	1.851	285	5.691	549
P18	0.0739	3.7	0.0060	3.0	0.0029	2.8	0.0016	9.0	0.722	2.2	0.532	88.5	0.984	519	2.366	423
P20	0.0731	3.7	0.0059	3.0	0.0028	2.8	0.0024	8.0	0.721	4.4	0.476	54.5	0.992	48	2.650	157
P22	0.0724	3.6	0.0061	3.1	0.0022	2.2	0.0040	6.2	0.723	3.7	0.458	17.9	0.997	192	1.876	182
P24	0.0717	3.6	0.0055	2.8	0.0035	3.5	0.0049	7.5	0.728	2.0	0.542	94.1	0.406	294	2.002	107
P26	0.0711	3.6	0.0056	2.8	0.0028	2.7	0.0064	9.7	0.733	5.4	0.664	25.3	-0.070	228	1.593	67
P28	0.0704	3.5	0.0050	2.5	0.0039	3.9	0.0069	10.5	0.738	5.3	0.627	16.5	0.365	92	1.555	40
P30	0.0700	3.5	0.0054	2.7	0.0030	2.9	0.0076	11.6	0.737	6.0	0.595	21.6	0.383	189	1.496	76
P32	0.0695	3.5	0.0052	2.6	0.0033	3.2	0.0086	13.2	0.732	1.9	0.412	186.2	1.026	874	1.358	44
P34	0.0690	3.5	0.0053	2.7	0.0025	2.4	0.0089	13.8	0.745	6.6	0.510	65.9	0.650	349	1.527	111
P36	0.0684	3.4	0.0048	2.4	0.0035	3.4	0.0087	13.2	0.744	1.0	0.549	118.9	0.535	432	1.498	32
P38	0.0680	3.4	0.0051	2.5	0.0023	2.2	0.0093	14.0	0.740	2.2	0.334	85.5	1.352	411	1.362	349
P40	0.0676	3.4	0.0048	2.4	0.0033	3.2	0.0100	15.4	0.744	0.5	0.514	78.9	0.372	656	1.184	205
P42	0.0670	3.4	0.0042	2.1	0.0047	4.7	0.0111	16.9	0.756	5.9	0.954	72.6	-1.170	526	1.252	394
P44	0.0667	3.3	0.0046	2.3	0.0033	3.2	0.0105	16.3	0.730	4.4	0.214	147.1	1.798	282	0.978	368
P46	0.0661	3.3	0.0043	2.1	0.0033	3.3	0.0107	15.8	0.734	5.8	-0.319	347.0	3.393	473	1.653	131
P48	0.0659	3.3	0.0047	2.3	0.0023	2.2	0.0107	16.7	0.743	11.7	0.409	9.8	1.389	39	1.284	424
P50	0.0655	3.3	0.0044	2.2	0.0036	3.5	0.0108	16.4	0.726	5.9	0.924	180.8	0.231	998	2.510	475

Table 2: The same as Table 1 but for air-broadened CO₂.

References

- [1] Buchwitz M, de Beek R, Burrows JP, Bovensmann H, Warneke T, Notholt J, Meirink JF, Goede APH, Bergamaschi P, Korner S, Heimann M, Schulz A. Atmospheric methane and carbon dioxide from SCIAMACHY stallite data: initial comparison with chemistry and transport models. *Atmos Chem Phys* 2005;5:941-62.
- [2] Butz A, Guerlet S, Hasekamp O, Schepers D, Galli A, Aben I, Frankenberg C, Hartmann JM, Tran H, Kuze A, Keppel-Aleks G, Toon G, Wunch D, Wennberg P, Deutscher N, Griffith D, Macatangay R, Messerschmidt J, Notholt J, Warneke T. Toward accurate CO₂ and CH₄ observations from GOSAT. *Geophys Res Lett* 2011;38:L14812, doi:10.1029/2011GL047888.
- [3] Crisp D. Measuring atmospheric carbon dioxide from space with the Orbiting Carbon Observatory-2 (OCO-2). *Proc SPIE* 9607, *Earth Observing Systems XX*, 9607072, 2015 <https://doi.org/10.1117/12.2187291>
- [4] Wunch D, Wennberg PO, Osterman G, Fisher B, Naylor B et al. Comparisons of the Orbiting Carbon Observatory-2 (OCO-2) xCO₂ measurements with TCCON. *Atmos Meas Tech* 2017;10:2209-38.
- [5] Miller CE, Brown LR, Toth RA, Benner DC, Malathy DV. Spectroscopic challenges for high accuracy retrievals of atmospheric CO₂ and the Orbiting Carbon Observatory (OCO) experiment. *C R Phys Acad Sci Paris* 2005;6:876-87.
- [6] Miller CE, Crisp D, DeCola PL, Olsen SC, Randerson JT, Michalak AM et al. Precision requirements for space-based xCO₂ data. *J Geophys Res*, 2007;112:D10314, doi:10.1029/2006JD007659.
- [7] Hartmann JM, Tran H, Armante R, Boulet C, Campargue A, Ciurylo R, Forget F, Gianfrani L, Gordon I, Guerlet S, Gustafsson M, Hodges J, Kassi S, Lisak D, Thibault F, Toon GC. Recent advances in collisional effects on spectra of molecular gases and their practical consequences. *J Quant Spectrosc Radiat Transfer* 2018;213:178-227.
- [8] Long DA, Bielska K, Lisak D, Havey DK, Okumura M, Miller CE, Hodges JT. The air-broadened, near-infrared CO₂ line shape in the spectrally isolated regime: Evidence of simultaneous Dicke narrowing and speed dependence. *J Chem Phys* 2011;135:064308.
- [9] Bui TQ, Long DA, Cygan A, Sironneau VT, Hogan DW, Rupasinghe PM, Ciurylo R, Lisak D, Okumura M. Observations of Dicke narrowing and speed dependence in air-broadened CO₂ lineshapes near 2.06 μm. *J Chem Phys* 2014;141:174301.
- [10] Lin H, Reed ZD, Sironneau VT, Hodges JT. Cavity ring-down spectrometer for high-fidelity molecular absorption measurements. *J Quant Spectrosc Radiat Transf* 2015;161:11-20.
- [11] Long DA, Wojtewicz S, Miller CE, Hodges JT. Frequency-agile, rapid scanning cavity ring-down spectroscopy (FARS-CRDS) measurements of the (30012)←(00001) near-infrared carbon dioxide band. *J Quant Spectrosc Rad Transf* 2015;161:35-40.
- [12] Benner DC, Devi VM, Sung K, et al. Line parameters including temperature dependences of air- and self-broadened line shapes of ¹²C¹⁶O₂: 2.06-μm region. *J Mol Spectrosc* 2016;326:31-47.
- [13] Ghysels M, Liu Q, Fleisher AJ, Hodges JT. A variable-temperature cavity ring-down spectrometer with application to line shape analysis of CO₂ spectra in the 1600 nm region. *Appl Phys B* 2017;123-124:1-13.
- [14] Wilzewski JS, Birk M, Loos J, Wagner G. Temperature-Dependence Laws of Absorption Line Shape Parameters of the CO₂ ν₃ Band. *J Quant Spectrosc Rad Transfer* 2018;206:296-305.
- [15] Benner DC, Rinsland CP, Devi VM, Smith MAH, Atkins D. A multispectrum nonlinear least squares fitting technique. *J Quant Spectrosc Radiat Transfer* 1995;53:705-21.
- [16] Nguyen HT, Ngo NH, Tran H. Prediction of line shape parameters and their temperature dependences for CO₂-N₂ using molecular dynamics simulations. *J Chem Phys* 2018;149:224301.

- [17] Tran DD, Sironneau VT, Hodges JT, Armante R, Cuesta J, Tran H. Prediction of high-order line-shape parameters for air-broadened O₂ lines using requantized classical molecular dynamics simulations and comparison with measurements. *J Quant Spectrosc Rad Transfer* 2019;222-223:108-14.
- [18] Hartmann JM, Tran H, Ngo NH, Landsheere X, Chelin P, Lu Y, Liu AW, Hu SM, Gianfrani L, Casa G, Castrillo A, Lepère M, Delière Q, Dhyne M, Fissiaux L. Ab initio calculations of the spectral shapes of CO₂ isolated lines including non-Voigt effects and comparisons with experiments. *Phy Rev A* 2013;87:013403.
- [19] Larcher G, Tran H, Schwell M, Chelin P, Landsheere X, Hartmann JM. CO₂ isolated line shapes by classical molecular dynamics simulations: influence of the intermolecular potential and comparison with new measurements. *J Chem Phys* 2014;140:084308.
- [20] Hartmann JM, Sironneau V, Boulet C, Svensson T, Hodges JT, Xu CT. Collisional broadening and spectral shapes of absorption lines of free and nanopore-confined O₂ gas. *Phys Rev A* 2013;87:032510. doi:10.1103/PhysRevA.87.032510.
- [21] Lamouroux J, Sironneau V, Hodges JT, Hartmann JM. Isolated line shapes of molecular oxygen: Requanted classical molecular dynamics calculations versus measurements. *Phys Rev A* 2014;89:042504. doi:10.1103/PhysRevA.89.042504.
- [22] Ngo NH, Tran H, Gamache RR, Bermejo D, Doménech JL. Influence of velocity effects on the shape of N₂ (and air) broadened H₂O lines revisited with classical molecular dynamics simulations. *J Chem Phys* 2012;137:064302.
- [23] Ngo NH, Tran H, Gamache RR. Pure H₂O isolated line-shape modeling based on classical molecular dynamics simulations of velocity changes and semi-classical calculations of the speed-dependent collisional parameters. *J Chem Phys* 2012;136:154310.
- [24] Tran H, Ngo NH, Hartmann JM, Gamache RR, Mondelain D, Kass S, Campargue A, Gianfrani L, Castrillo A, Rohart F. Velocity effect on the shape of pure H₂O isolated lines: Complementary tests of the partially-Correlated Speed-Dependent Keilson-Storer model. *J Chem Phys* 2013;138:034302.
- [25] Le T, Domenech JL, Lepère M, Tran H. Molecular dynamic simulations of N₂-broadened methane line shapes and comparison with experiments. *J Chem Phys* 2017;146,094305.
- [26] Tran H, Domenech JL. Spectral shapes of Ar-broadened HCl lines in the fundamental band by classical molecular dynamics simulations and comparison with experiments. *J Chem Phys* 2014;141:064313.
- [27] Ngo NH, Hartmann JM. A strategy to complete databases with parameters of refined line shapes and its test for CO in He, Ar and Kr. *J Quant Spectrosc Radiat Transf* 2017;203:334–40. doi:10.1016/j.jqsrt.2017.01.031.
- [28] Murthy CS, O’Shea SF, McDonald IR. Electrostatic interactions in molecular crystals lattice dynamics of solid nitrogen and carbon dioxide. *Mol Phys* 1983;50:531-41.
- [29] Bouanich JP. Site-site Lennard-Jones potential parameters for N₂, O₂, H₂, CO and CO₂. *J Quant Spectrosc Radiat Transfer* 1992;47:243-50.
- [30] Hirschfelder JE, Curtiss CF, Bird RB, *Molecular Theory of Gases and Liquids* (Wiley, New York, 1954).
- [31] Rosenkranz PK. Shape of the 5 mm oxygen band in the atmosphere. *IEEE Trans Antennas Propag* 1975;23:498-506.
- [32] Ngo NH, Lisak D, Tran H, Hartmann JM. An isolated line-shape model to go beyond the Voigt profile in spectroscopic databases and radiative transfer codes. *J Quant Spectrosc Rad Transf* 2013;129:89-100.
- [33] Rohart F, Mader H, Nicolaisen HW. Speed dependence of rotational relaxation induced by foreign gas collisions: studies on CH₃F by millimeter wave coherent transients. *J Chem Phys* 1994;101:6475-86.

- [34] Rohart F, Ellendt A, Kaghat K, Mäder H. Self and polar foreign gas line broadening and frequency shifting of CH₃F: effect of the speed dependence observed by millimeter-wave coherent transients. *J Mol Spectrosc* 1997;185:222-33.
- [35] Nelkin M, Ghatak A. Simple binary collision model for Van Hove's G_s(r,t), *Phys Rev* 1964;135:A4-A9.
- [36] Rautian SG, Sobel'man II. The effect of collisions on the Doppler broadening of spectral lines. *Sov Phys Usp* 1967;9:701-16.
- [37] Delahaye T, Maxwell SE, Reed ZD, Lin H, Hodges JT, Sung K, Devi VM, Warneke T, Spietz P, Tran H. Precise methane absorption measurements in the 1.64 μm spectral region for the MERLIN mission. *J Geophys Res Atmos* 2016;121:7360-70.
- [38] Ngo NH, Lin H, Hodges JT, Tran H. Spectral shapes of rovibrational lines of CO broadened by He, Ar, Kr and SF₆: A test case of the Hartmann-Tran profile. *J Quant Spectrosc Rad Transfer* 2017;203:325-333.
- [39] Tennyson J, Bernath PF, Campargue A, Csaszar AG, Daumont L, Gamache RR, Hodges JT, Lisak D, Naumenko OV, Rothman LS, Tran H, Zobov NF, Buldyreva J, Boone CD, De Vizia MD, Gianfrani L, Hartmann JM, McPheat R, Weidmann D, Murray J, Ngo NH, Polyansky OL. Recommended isolated-line profile for representing high-resolution spectroscopic transitions (IUPAC technical report). *Pure App Chem* 2014;86:1931-43.
- [40] Devi VM, Benner DC, Miller CE, Predoi-Cross A. Lorentz half-width, pressure-induced shift and speed-dependent coefficients in oxygen-broadened CO₂ bands at 6227 and 6348 cm⁻¹ using a constrained multispectrum analysis. *J Quant Spectrosc Rad Transf* 2010;111:2355-69.
- [41] Hikida T, Yamada KMT. N₂- and O₂-broadening of CO₂ for the (300 1)III ← (0000) band at 6231 cm⁻¹. *J Mol Spectrosc* 2006;239:154-9.
- [42] Devi VM, Benner DC, Sung K, Brown LR, Crawford TJ, Miller CE, Drouin BJ, Payne VH, Yu S, Smith MAH, Mantz AW, Gamache RR. Line parameters including temperature dependences of self- and air-broadened line shapes of ¹²C¹⁶O₂: 1.6 μm region. *J Quant Spectrosc Rad Transf* 2016;177:117-44.
- [43] Lisak D, Cygan A, Bermejo D, Domenech JL, Hodges JT, Tran H. Application of the Hartmann–Tran profile to analysis of H₂O spectra. *J Quant Spectrosc Rad Transf* 2015;164:221-30.
- [44] Gordon IE, Rothman LS, Hill C, Kochanov RV, Tan Y, Bernath PF, Birk M, Boudon, Campargue A, Chance KV, Drouin BJ, Flaud JM, Gamache RR, Hodges JT, Jacquemart D, Perevalov VI, Perrin A, Shine KP, Smith MAH, Tennyson J, Toon GC, Tran H, Tyuterev VG, Barbe A, Császár AG, Devi VM, Furtenbacher T, Harrison JJ, Hartmann J-M, Jolly A, Johnson TJ, Karman T, Kleiner I, Kyuberis AA, Loos J, Lyulin OM, Massie ST, Mikhailenko SN, Moazzen-Ahmadi N, Müller HSP, Naumenko OV, Nikitin AV, Polyansky OL, Rey M, Rotger M, Sharpe SW, Sung K, Starikova E, Tashkun SA, Vander Auwera J, Wagner G, Wilzewski J, Wcisło P, Yu S, Zak EJ. The HITRAN2016 molecular spectroscopic database. *J Quant Spectrosc Radiat Transf* 2017;203:3–69. doi:10.1016/j.jqsrt.2017.06.038.
- [45] Le T, Fissiaux L, Lepere M, Tran H. Isolated line shape of methane with various collision partners. *J Quant Spectrosc Rad Transf* 2016 ;185 :27-36.
- [46] Tran DD, Tran H, Vasilchenko S, Kassi S, Campargue A, Mondelain D. High sensitivity spectroscopy of the O₂ band at 1.27 μm: (II) air-broadened line profile parameters. *J Quant Spectrosc Rad Transf* 2019, in revision.
- [47] Hartmann JM, Boulet C, Robert D. *Collisional effects on molecular spectra. Laboratory experiments and model, consequences for applications*. Elsevier, Amsterdam 2008.
- [48] Lamouroux J, Régalia L, Thomas X, Vander Auwera J, Gamache RR, Hartmann JM. CO₂ line-mixing database and software update and its tests in the 2.1 μm and 4.3 μm regions. *J Quant Spectrosc Rad Transfer* 2015;151:88-96.

[49] Predoi-Cross A, Liu W, Holladay C, Unni AV, Schofield I, McKellar ARW, Hurtmans D. Line profile study of transitions in the 30012←00001 and 30013←00001 bands of carbon dioxide perturbed by air. *J Mol Spectrosc* 2007;246:98-112.